

Impact of calibration errors on CMB component separation using FastICA and ILC

Jason Dick^{1*}, Mathieu Remazeilles^{2,3†}, Jacques Delabrouille^{2‡}

¹ *SISSA via Beirut, 2-4, 34014 Trieste, Italy*

² *APC 10, rue Alice Domon et Léonie Duquet, 75205 Paris Cedex 13, France*

³ *Laboratoire de Physique Théorique, Université Paris-Sud, 91405 Orsay, France*

Submitted to MNRAS 2009 July 17

ABSTRACT

The separation of emissions from different astrophysical processes is an important step towards the understanding of observational data. This topic of component separation is of particular importance in the observation of the relic Cosmic Microwave Background Radiation, as performed by the WMAP satellite and the more recent Planck mission, launched May 14th, 2009 from Kourou and currently taking data. When performing any sort of component separation, some assumptions about the components must be used. One assumption that many techniques typically use is knowledge of the frequency scaling of one or more components. This assumption may be broken in the presence of calibration errors. Here we compare, in the context of imperfect calibration, the recovery of a clean map of emission of the Cosmic Microwave Background from observational data with two methods: FastICA (which makes no assumption of the frequency scaling of the components), and an ‘Internal Linear Combination’ (ILC), which explicitly extracts a component with a given frequency scaling. We find that even in the presence of small calibration errors with a Planck-style mission, the ILC method can lead to inaccurate CMB reconstruction in the high signal-to-noise regime, because of partial cancellation of the CMB emission in the recovered map. While there is no indication that the failure of the ILC will translate to other foreground cleaning or component separation techniques, we propose that all methods which assume knowledge of the frequency scaling of one or more components be careful to estimate the effects of calibration errors.

Key words: cosmology: theory – cosmology: observation

1 INTRODUCTION

Precise observation of the Cosmic Microwave Background (CMB), as planned with the Planck space mission (Bersanelli & Mandolesi, 2000; Lamarre et al., 2000; Tauber, 2004), is of the utmost importance for better understanding, and confronting with precise observational data, the hot big bang model and its theoretical predictions. In this theoretical framework, such observations also permit constraining the parameters of the model, as is currently done to a lesser extent by a number of previous experiments, such as COBE (Fixsen et al., 1997), WMAP (Komatsu et al., 2009), ACBAR (Reichardt et al., 2009), Archeops (Benoît et al., 2003; Tristram et al., 2005), BOOMERANG (MacTavish et al., 2006), CBI (Sievers et al., 2009), QUaD (QUaD col-

laboration: C. Pryke et al., 2008), and VSA (Rebolo et al., 2004).

With ever more sensitive instruments, the main source of uncertainty in CMB observations, rather than being instrumental noise, is the contamination of the observation by foreground emission. Astrophysical foregrounds comprise millimeter wave emission from the interstellar medium in our own galaxy, as well as emission from compact extragalactic sources.

Component separation methods make use of the different emission laws of different astrophysical components to separate them through joint analysis of observations made at different wavelengths (Delabrouille & Cardoso, 2007). Among those methods, the so-called Internal Linear Combination (ILC), which makes few assumptions about the physical properties of the CMB and the foregrounds, has been widely used for the analysis of WMAP data (Tegmark et al., 2003; Eriksen et al., 2004; Delabrouille et al., 2009; Kim et al., 2009). An important assumption of the ILC is that

* E-mail: dick@sissa.it

† E-mail: remazeil@apc.univ-paris7.fr

‡ E-mail: delabrouille@apc.univ-paris7.fr

the frequency scaling of the CMB is assumed to be known. This is, in principle, a safe assumption, as small temperature fluctuations ΔT of the CMB generate brightness fluctuations proportional to ΔT , which scale in frequency like the derivative of a blackbody with respect to the temperature, at the well measured CMB temperature of $T = 2.725$ K. However, calibration coefficients for each channel, which are a multiplicative factor for each frequency, introduce an uncertainty in the frequency scalings of the CMB component in presence of calibration errors. For space-based missions these uncertainties are typically small (well below 1% for WMAP or Planck).

More sophisticated methods for component separation have been extensively studied in the community of statistical signal processing for a variety of applications. These methods are part of a field of activity generically designated as Blind Source Separation (BSS), or equivalently Independent Component Analysis (ICA). ICA methods perform separation on the basis of the assumption that each of the available observations is a different linear mixture of a well defined number of statistically independent components. Such methods generically rely on no prior assumption on the scaling coefficients of the components in the different available observations (i.e. on the coefficients of each component in the ‘mixtures’). In fact, recovering these coefficients (the so-called ‘mixing matrix’) is precisely the primary target of blind source separation. ICA methods, thus, do not typically assume perfect knowledge of the response of each channel to the CMB – nor that the CMB contribution is the same in all channels. For CMB studies particularly, this type of approach has led to the development of a large variety of methods, including CCA (Bonaldi et al., 2006; Bedini et al., 2005), FastICA (Hyvärinen, 1999), SMICA (Delabrouille et al., 2003; Cardoso et al., 2008) and GMCA (Bobin et al., 2008). These methods have been used on real observational data in a variety of contexts (Bonaldi et al., 2007; Maino et al., 2006; Patanchon et al., 2005), and compared extensively on simulated data sets (Leach et al., 2008).

The two main differences between the ILC and ICA methods are the following:

- Whereas ICA is designed to extract the scaling coefficients of each of the identified components from the data themselves, the ILC assumes perfect knowledge of the scaling coefficients for the component of interest (CMB);
- The ILC does not make any assumption about the properties of foreground contamination, whereas ICA assumes that the data are satisfactorily described by a (noisy) linear mixture of independent components.

Clearly, these methods are bound to be more or less adapted to component separation, depending upon the actual properties of the data set and on the science objectives pursued. In the following we propose to investigate, using realistic simulations of sky emission and of observational data for WMAP and Planck, the relative performance of FastICA and ILC in the presence of calibration errors. Such calibration errors result in the violation of one of the assumptions of the ILC (the prior knowledge of the exact scaling coefficients of the CMB in the observations). By contrast, blind component separation methods are designed from first principles to estimate the scaling coefficients from the data, and

in principle should not suffer much from calibration uncertainties.

The rest of this paper is organized as follows. In section 2 we describe the ILC and ICA component separation methods. We describe our methodology for comparing the methods in section 3. In section 4 we present the results of our analysis, followed by our conclusions in section 5. We also provide a detailed calculation of the effect of calibration errors on the ILC in the appendix A.

2 ILC AND ICA

In the following we assume that the available data (maps $x_i(p)$ of observed sky) can be written as

$$x_i(p) = a_i s(p) + n_i(p), \quad (1)$$

where $s(p)$ is the map of the component of interest (the CMB), p indexes pixels in the map, and $n_i(p)$ is the contribution from foregrounds and instrumental noise to the map $x_i(p)$. The coefficients a_i scale the relative amplitude of the CMB map in the different available observations. For observations in thermodynamic units, and perfect calibration, we have $\forall i, a_i = 1$.

2.1 The ILC

The philosophy behind the ILC is to find the linear combination of the available maps x_i which has minimal variance while retaining unit response to the CMB map. This linear combination, $\sum_i w_i x_i(p)$, is then an estimate $\hat{s}(p)$ of the true CMB map $s(p)$. The ILC weights w_i are found by solving the problem of minimizing $\text{var} \sum_i w_i x_i(p)$ under the constraint $\sum_i w_i = 1$. In principle, this last constraint guarantees unit response to the CMB, as we have:

$$\begin{aligned} \hat{s}(p) &= \sum_i w_i x_i(p) \\ &= s(p) + \sum_i w_i n_i(p). \end{aligned} \quad (2)$$

In the presence of foregrounds, which induce correlated errors from channel to channel, the ILC weights adjust themselves so that the linear combination cancels out as much of the foregrounds as possible. The actual weights, however, result from a trade-off between canceling foregrounds and allowing errors due to instrumental noise in the final map.

The constrained minimization problem can be solved in a straightforward manner using a Lagrange multiplier method to impose $\sum_i w_i = 1$. The resulting weights are found to be:

$$\mathbf{w} = \frac{\hat{\mathbf{R}}^{-1} \mathbf{a}}{\mathbf{a}^t \hat{\mathbf{R}}^{-1} \mathbf{a}}, \quad (3)$$

where $\hat{\mathbf{R}}$ is the empirical covariance matrix of the observations. Note that we have used bold font to denote vectors, and have omitted the reference to the pixel value. From here on, this notation will be used. The ILC estimator of the CMB map $s(p)$ can be written as:

$$\hat{s}_{\text{ILC}} = \mathbf{w}^t \mathbf{x} = \frac{\mathbf{a}^t \hat{\mathbf{R}}^{-1} \mathbf{x}}{\mathbf{a}^t \hat{\mathbf{R}}^{-1} \mathbf{a}}. \quad (4)$$

The ILC weights, obviously, depend upon the assumed scaling coefficients a_i for the component of interest. It is then clear that an error in the assumed scalings changes the ILC performance, but by how much? As the ILC attempts to minimize the total variance of the output map, the constraint that $\sum w_i a_i = 1$ plays a critical role in guaranteeing that the linear combination does not adjust its coefficients to cancel the CMB as well as foregrounds. It is foreseeable, then, that calibration errors could, in some cases, impact the performance of ILC more severely than just a small overall calibration error on the final output map.

2.2 FastICA

There is a wide choice of possible ICA methods to extract the CMB from multifrequency observations. In this paper, we make use of the standard FastICA algorithm as described in Hyvärinen (1999), with a few minor changes:

- We subtract an estimate of the instrument noise covariance matrix from the empirical covariance matrix of the data.
- Instead of leaving the estimated signal as being unit variance, we set the CMB scaling to be such that the sum of the weights is equal to one, mirroring the ILC method to ensure unit response to the CMB.

FastICA is based on the general principle that a sum of two different independent probability distributions will always tend to be more Gaussian than either of the distributions are independently. We can thus extract N independent sources from N channels of data by forming the linear combination of the N channels which maximizes the non-Gaussianity of the extracted sources. A measure of the non-Gaussianity of each source is performed using functions such as:

$$Y(x) \propto [E\{G(x)\} - E\{G(y)\}]^2. \quad (5)$$

where x is data that has unit variance, and y is a random variable drawn from a unit-variance Gaussian distribution. Here $E\{\}$ is the expectation value of the data set or probability distribution enclosed and $G(x)$ is some non-linear function. Popular choices include a Gaussian, a polynomial, or the logarithm of the hyperbolic cosine. Which specific choice is best depends upon precisely how the distribution of x differs from a Gaussian, though it is clear that for any choice of $G(x)$, $Y(x)$ will be zero if x is Gaussian-distributed, and positive definite otherwise. In the present paper, we use $G(x) = x^4$.

FastICA assumes a model of the data of the form :

$$\mathbf{x} = \mathbf{A}\mathbf{s} + \mathbf{n}, \quad (6)$$

where now vector \mathbf{s} comprises all ‘sources’ (CMB + foregrounds), and \mathbf{n} is instrumental noise only (for all channels). The objective of the method is to evaluate the mixing matrix \mathbf{A} , and then use this estimate to invert the linear system.

In order to optimize estimation of the mixing matrix that determines the linear combination of x which represents the individual sources, FastICA also performs a pre-whitening step. This pre-whitening step exploits the assumption of statistical independence to perform a linear

transformation on the data, which sets its covariance matrix to the identity by multiplying the data by the inverse square root of its covariance. The mixing matrix then becomes a simple rotation matrix which, with its smaller number of degrees of freedom, is easier to estimate.

For generating the pre-whitening matrix, we do not make direct use of the covariance matrix of the data, as with basic FastICA, but instead use the estimated covariance matrix of the signal as in Maino et al. (2002). This can be understood simply by our modeling of the data (equation 6). Given this data model, the covariance of the observations is:

$$\begin{aligned} \mathbf{R}_x &= \langle (\mathbf{A}\mathbf{s} + \mathbf{n})(\mathbf{A}\mathbf{s} + \mathbf{n})^t \rangle \\ \mathbf{R}_x &= \mathbf{A}\mathbf{R}_s\mathbf{A}^t + \mathbf{R}_n. \end{aligned} \quad (7)$$

Here the correct covariance matrix to use to whiten the signal is $\mathbf{A}\mathbf{R}_s\mathbf{A}^t$, which we estimate as $\mathbf{R}_x - \mathbf{R}_n$. The channel-channel noise covariance \mathbf{R}_n is taken as diagonal with the diagonal elements estimated from our knowledge of the per-pixel noise in each map combined with how much each map was smoothed. We have assumed that the signal and noise are uncorrelated in the above derivation.

Having performed the pre-whitening, all extracted sources have unit variance and are uncorrelated. To determine the overall CMB scaling, we first determine which of the sources is the CMB, then use the ILC strategy of setting the sum of the CMB weights equal to one. This ensures that the level of the CMB in the output is, at least in the case of no calibration error, equal to the level of the CMB in the maps.

3 METHOD

We now turn to the investigation of the impact of calibration errors on component separation with ILC and FastICA. The approach of this investigation consists of generating simulated ‘observations’, with varying calibration errors, noise levels, and frequency channels, and compare the performance of ILC and FastICA at recovering the CMB map.

Performance is measured in several ways, based on the measurement of reconstruction errors of different types.

Denoting as $s(p)$ the (beam-smoothed) CMB map used in the simulation, and as $\hat{s}(p)$ the CMB map obtained from processing the simulated data, the reconstruction error is $\hat{s}(p) - s(p)$.

This reconstruction error arises from two terms. A multiplicative term (i.e. a global calibration error) and an additive term. We have

$$\hat{s}(p) = \alpha s(p) + c(p)$$

where α is the global calibration coefficient, and $c(p)$ the additive contamination by foregrounds and noise. Ideally, we aim at $\alpha = 1$ and $c(p) = 0$.

In practice, in both ILC and ICA methods, the final map is reconstructed as a linear combination $\sum w_i x_i(p)$ of the input maps $x_i(p)$. Hence, for simulated data, one can compute easily $\alpha = \sum w_i a_i$ and $c(p) = \sum w_i n_i(p)$, where $n_i(p)$ are maps of the sum noise and foregrounds in channel i .

The comparison of the variance of the reconstruction error, of the overall response α , and of the contamination $c(p)$

for ILC and ICA gives insight on the relative performance of the two, and of the main origin of error, in presence of calibration uncertainties.

3.1 Simulations

In preparation for the forthcoming Planck space mission, simulations for the 9 Planck frequency channels, from 30 to 857 GHz, as described in the Planck 'Bluebook'¹, are made. We also consider simulations in the WMAP frequency channels, between 23 and 94 GHz. Sky simulations are performed using the Planck Sky Model (PSM) package, version 1.6.3² and using the Healpix pixelization. In the simulated observations, we introduce a small calibration error, so that each of the sky maps is multiplied by a calibration coefficient. We consider calibration errors $\delta a/a$ of 0.1, 0.2, 0.5, and 1%, which implies calibration coefficients typically somewhere between 0.99 and 1.01.³ We work at the resolution of the lowest frequency channel in our simulations, i.e. 33 arcminute beams for Planck, and 54 arcminute beams for WMAP.

Noise compatible with what is expected for the two instruments, for maps smoothed at the resolution of the lowest frequency channel, is added to the sky emission. We then separate components with both an ILC and with FastICA, and analyze and interpret the results.

3.1.1 Planck Sky Model

Sky maps are generated using a four-component model of galactic emission which includes free-free, synchrotron, thermal dust, and spinning dust diffuse components. We also add emission from several populations of compact sources, which comprise ultracompact galactic H-II regions, infra-red and radio sources (both galactic and extragalactic), a far infrared background emission, and thermal SZ effect from a simulated distribution of galaxy clusters. For our Planck simulations, maps are generated at 30GHz, 44GHz, 70GHz, 100GHz, 143GHz, 217GHz, 353GHz, 545GHz, and 857GHz, each at $n_{\text{side}}=1024$. For WMAP simulations, maps are generated at 23GHz, 33GHz, 41GHz, 61GHz, and 94GHz, each at $n_{\text{side}}=512$. Maps are simulated using Gaussian symmetric beams. Only temperature maps are generated.

3.1.2 Post-processing of PSM Outputs

Instrumental noise is added separately after the sky is simulated with the PSM. For Planck, we assume uniform sky coverage, with noise level corresponding to what is given in the Planck 'Bluebook'. Since the FastICA and ILC methods require maps that are at the same resolution, we then smooth all maps to the resolution of the 30GHz channel, which has a Gaussian beam FWHM of 33'. As we use a relatively low resolution beam, all maps are set to $n_{\text{side}}=512$ after smoothing.

After adding noise and smoothing maps to the same resolution, we simulate the calibration error by drawing a

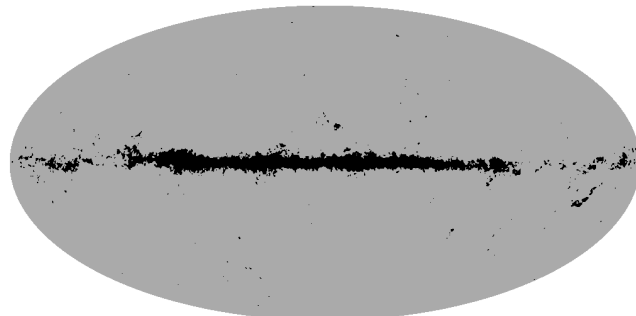


Figure 1. Mask that removes the brightest pixels from the 70GHz and 100GHz channels.

zero-mean Gaussian random variable x with RMS equal to the desired calibration error (e.g. $\sigma = 0.002$ for 0.2% error). We then multiply the map by $1+x$. This is repeated for each frequency channel, with the same calibration RMS error but a different realization of x for each.

While it makes no difference whether the calibration error simulation is performed before or after smoothing, we note that it is correct to add the calibration error after the noise, as the overall estimated noise level also depends upon the calibration of the instrument. As we make use of the estimated noise covariance between the channels, the estimated noise level after smoothing is also computed here.

3.2 Masking

For better performance of the FastICA or ILC component separation algorithms, it is safer to mask out particularly bright sources as well as those with strongly-varying spectral properties. The mask is determined making use of a simple magnitude-based algorithm. First, we produce a theoretical estimate of the expected CMB RMS based upon the WMAP power spectrum. We then generate a mask that removes all pixels which contain a value larger than four times the CMB RMS.

For our maps, the mask used is a union of the masks computed as above from the 70GHz and 100GHz channels. We make use of the mask as generated from the first realization with no calibration error, and do not recompute the mask between runs. The resultant mask is shown in fig. 1. It is possible that we could obtain better component separation performance through more precise masking, but this is not expected to have any impact on the overall results of the present paper. The study could have been performed with any arbitrary mask, as long as the average CMB to foreground ratio is not changed significantly.

3.3 Monte Carlo

In order to investigate both the average of the reconstruction error and its dispersion, we individually execute each of the above steps many times for each chosen set of parameters, the exact number depending upon the test. Summary statistics are then computed across the runs. When comparing different component separation techniques, the exact same set of realizations are used. Different choices of the calibration error level also make use of the same input sky maps.

¹ [http://www.rssd.esa.int/SA/PLANCK/docs/Bluebook-ESA-SCI\(2005\)1_V2.pdf](http://www.rssd.esa.int/SA/PLANCK/docs/Bluebook-ESA-SCI(2005)1_V2.pdf)

² <http://www.apc.univ-paris7.fr/APC-CS/Recherche/Adamis/PSM/psky-en.php>

³ The calibration error expected for Planck is less than 1% up to the 353GHz channel, as given by the Planck 'Bluebook'

For these simulations, CMB and noise are generated from their statistical properties separately in each simulation. The CMB is a Gaussian realization assuming, for all simulations, the same power spectrum, compatible with WMAP best fit model, but new phases for each realization. Similarly, all realizations of noise are independent.

Other components are not fully independent from realization to realization. Galactic components, the model of which is heavily constrained by WMAP observations, do not change much. The Sunyaev Zel'dovich map is fixed (i.e. the same SZ template map is used in all simulations). A fraction of point sources remain similar (they are based on the positions of real sources) although their spectral emission law depends on the realization. An additional population of point sources, generated to correct for the sky coverage of point source surveys to homogenize the point source distribution, is generated independently for each sky realization.

4 RESULTS

In this section we present both analytical and numerical results obtained after including the presence of calibration errors in the ILC and ICA component separation methods. The success or the failure of a method will be evaluated as follows. We construct the output CMB map estimates by ILC or ICA as well as the residual map, which is the difference map between the estimated output CMB map and the simulated input CMB map. We compute the RMS value of each of these maps and compare them. We also evaluate both the multiplicative factor α and the additive error $c(p)$ (introduced in section 3), characterizing the reconstruction errors.

4.1 Compared reconstruction error

The average root mean square of the reconstruction error $\hat{s} - s$, over all simulations for the Planck experiment, is computed in 10 bands of varying galactic latitude. The relative error, $r = E(s - \hat{s})/E(s)$, for both FastICA and the ILC, is plotted in figures 2 and 3.

As we expected, FastICA is almost completely unaffected by calibration errors. Because no assumption on the relative calibration is used, the overall calibration error just adds some small extra variance on the overall level of the extracted CMB.

ILC, however, is not so well behaved as FastICA. While ILC is somewhat better than FastICA at extracting the CMB when calibration is perfect, it quickly becomes worse as calibration errors of increasing magnitude are applied. Fig. 4 shows the output of a particular realization at 1% calibration error where ILC performed especially poorly, compared with the input CMB plotted on the same scale. The variance of the ILC output is much lower than the true CMB, and CMB features are strongly suppressed. As ILC attempts to find the minimum-variance output, it finds that with calibration errors it is possible to partially cancel the CMB to get the lowest possible variance output.

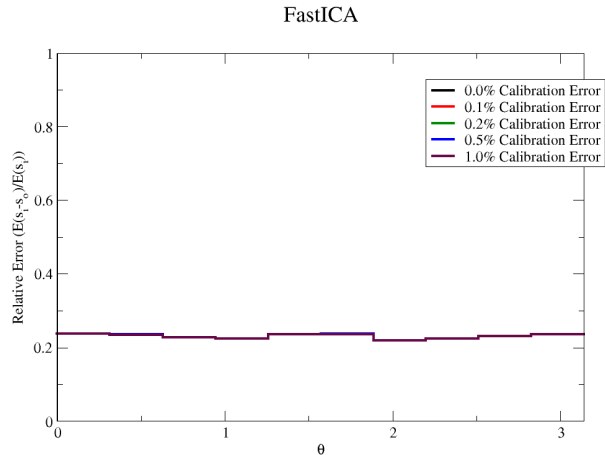


Figure 2. Plot of the relative error of FastICA as a function of galactic latitude. Generated using 128 simulations for each case. As expected, the relative error of FastICA has very little dependence upon the calibration error.

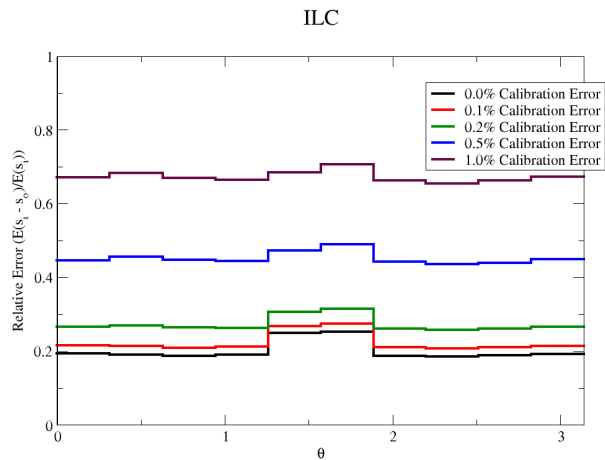


Figure 3. Plot of the relative error of ILC as a function of galactic latitude. Generated using 128 simulations for each case. Unlike FastICA, ILC shows tremendous sensitivity to the calibration error, causing a noticeable reduction in the quality of the extraction of the CMB even at the optimistic 0.1% calibration error level.

4.2 Interpretation of the ILC failure

The impact of calibration errors on ILC weights, and on the output CMB map, is analytically explored in Appendix A. Here we highlight that the signal-to-noise ratio plays a decisive role on this impact.

The ILC method is a linear combination of the maps observed in different frequency channels, $\hat{s} = \sum_i w_i x_i$. The ILC combination has minimum variance under the constraint

$$\sum_i w_i a_i = 1. \quad (8)$$

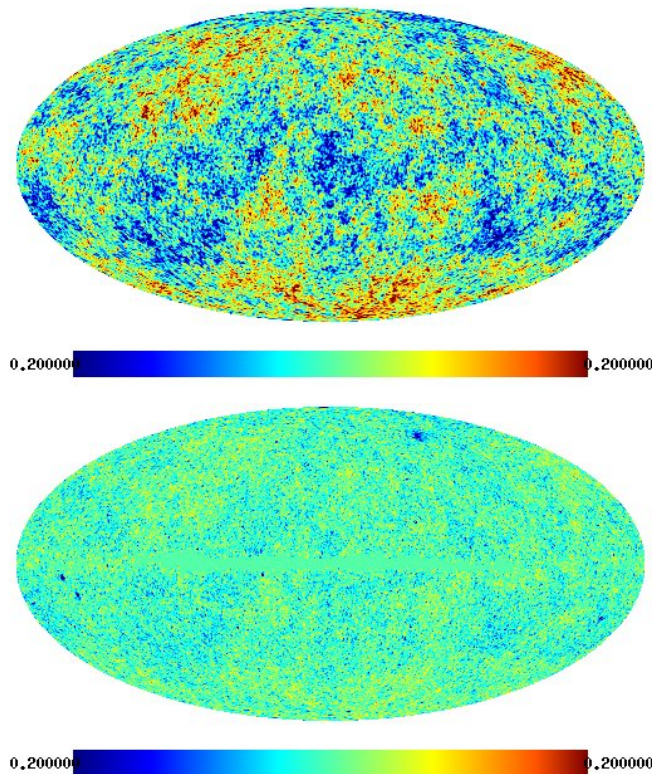


Figure 4. Input CMB and ILC-estimated CMB plotted on a 0.2mK scale for one realization at 1% calibration error with particularly bad output (relative error near 1.0). Note that the variance of the ILC output is far below the input CMB, indicating that the input CMB was largely canceled.

The constraint in principle guarantees the CMB conservation, otherwise $w_i = 0$ for all i would minimize the variance. If the calibration a_i is wrong then the CMB conservation is no longer guaranteed. In some cases, when the signal-to-noise ratio is large enough, it can be dramatic for the CMB extraction (see section 4.3).

As discussed above, the reconstruction error arises from two terms. A multiplicative term, i.e. a global calibration error term, and an additive contamination term. We can write the estimated CMB map as a function of the true CMB map as:

$$\hat{s}(p) = \alpha s(p) + c(p),$$

where α is the global calibration coefficient, and $c(p)$ the contamination by foregrounds and noise. Figure 5 shows this parameter α versus the input map calibration error. The presence of calibration errors δ_{a_i} modifies the calibration coefficients in each channel as $a_i \rightarrow a_i + \delta_{a_i}$, where $\delta_{a_i} \ll a_i$. We may explicitly expand the multiplicative error and the additive error in terms of the calibration errors δ_{a_i} and the ILC weights w_i :

$$\begin{aligned} \hat{s}(p) &= \sum_i w_i x_i(p) \\ &= \sum_i w_i (a_i + \delta_{a_i}) s(p) + \sum_i w_i n_i(p) \\ &= \left(1 + \sum_i w_i \delta_{a_i}\right) s(p) + \sum_i w_i n_i(p), \end{aligned} \quad (9)$$

CMB Calibration after Component Separation

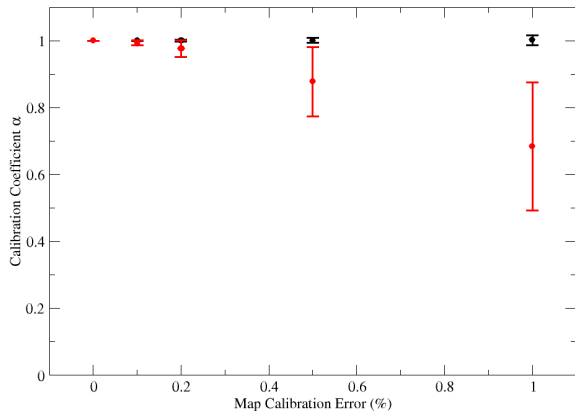


Figure 5. This figure shows the overall calibration coefficient of the output CMB map, computed from the known calibration errors in the inputs and the weights applied to obtain the output. The error bars represent the RMS of α among the 128 realizations. For FastICA, the calibration coefficient is centered very near one, with an RMS of approximately 1.5 times the map calibration error. By contrast, ILC has a CMB calibration that is perfect if the map calibration is perfect, but this quickly turns into a significant bias with large uncertainties as to the final calibration value.

where the ILC weights w_i satisfy the constraint $\sum_i w_i a_i = 1$. Thus we have

$$c(p) = \sum_i w_i n_i(p), \quad (10)$$

$$\alpha = 1 + \sum_i w_i \delta_{a_i}. \quad (11)$$

The additive error term $c(p) = \sum_i w_i n_i(p)$ is responsible for a bias in the CMB estimation because of foreground and noise contaminations even in the absence of calibration errors. Delabrouille et al. (2009) have explored the impact of this term on the ILC estimation of the CMB and have found that, in addition to the standard reconstruction error due to foreground and noise contamination, there is a bias, $E(s \cdot (\hat{s} - s))$, due to the estimation of second order statistics on samples of finite size. Both errors contribute to the variance of the output CMB map as

$$E(\hat{s}^2) = E(s^2) + E((\hat{s} - s)^2) + 2E(s \cdot (\hat{s} - s)).$$

The multiplicative error term $\alpha = 1 + \sum_i w_i \delta_i$ becomes non trivial in presence of calibration errors because the ILC weights w_i , as derived in equation (A6) of Appendix A, do not depend only on the calibration errors δ_{a_i} but also on the signal-to-noise ratio $\sigma^2 R_n^{-1}{}_{ij}$, where $\sigma^2 = E(s^2)$ and $(R_n)_{ij} = E(n_i n_j)$ denote respectively the variance of the CMB signal and the covariance matrix of the noise (including foregrounds).

4.3 Importance of the signal to noise ratio

From the exact expression (A6) of the weights we may write the multiplicative factor $\alpha = 1 + \mathbf{w}^t \boldsymbol{\delta}_a$ as

$$\alpha = \frac{\mathbf{a}^t \mathbf{R}_n^{-1} \mathbf{a} + \mathbf{a}^t \mathbf{R}_n^{-1} \boldsymbol{\delta}_a}{\mathbf{a}^t \mathbf{R}_n^{-1} \mathbf{a} + \sigma^2 [(\mathbf{a}^t \mathbf{R}_n^{-1} \mathbf{a})(\boldsymbol{\delta}_a^t \mathbf{R}_n^{-1} \boldsymbol{\delta}_a) - (\mathbf{a}^t \mathbf{R}_n^{-1} \boldsymbol{\delta}_a)^2]}. \quad (12)$$

The immediate consequence of equation (12) is the existence of two regimes.

If the signal-to-noise ratio is small enough compared to the inverse of the calibration error, typically,

$$\text{if } \sigma^2 \boldsymbol{\delta}_a^t \mathbf{R}_n^{-1} \boldsymbol{\delta}_a \ll 1 \text{ then } \alpha \approx 1 + \mathcal{O}(|\boldsymbol{\delta}_a|/|\mathbf{a}|),$$

because the expression proportional to σ^2 becomes negligible in (12). So we tend to recover the almost perfect CMB reconstruction close to the case of no calibration error ($\boldsymbol{\delta}_a = 0$).

If the signal-to-noise ratio becomes large enough then the reconstruction of the CMB signal may be dramatically damaged. This is the main result of this paper. Typically,

$$\text{if } \sigma^2 \boldsymbol{\delta}_a^t \mathbf{R}_n^{-1} \boldsymbol{\delta}_a \gg 1 \text{ then } \alpha \approx 0,$$

the multiplicative factor goes to zero since the expression proportional to σ^2 dominates all the other terms in (12), in which case the ILC estimation completely “kills” the expected CMB signal, $\hat{s}(p) \approx c(p)$.

Let us complete the discussion by relating the first and second moments of the output CMB \hat{s} and the reconstruction error $\hat{s} - s$ to the multiplicative and the additive errors. Considering that the CMB and the noise (including foregrounds) are independent random signals, $E(n_i s) = 0$, and assuming that $E(n_i) = 0$, we get

$$\begin{aligned} E(\hat{s} - s) &= (\alpha - 1)E(s), \\ E(s \cdot (\hat{s} - s)) &= (\alpha - 1)E(s^2), \\ E((\hat{s} - s)^2) &= (\alpha - 1)^2 E(s^2) + E(c(p)^2), \end{aligned} \quad (13)$$

where $E(c(p)^2) = \mathbf{w}^t \mathbf{R}_n \mathbf{w}$. The detailed expression of these moments in terms of the calibration errors and the signal-to-noise ratio is derived in Appendix A. From (13), once again, if the signal-to-noise is large enough then the reconstruction of the CMB is biased since α moves away from one to reach zero.

4.4 A simple example

Here we show a schematic description of the process using a simple example. We consider a two-channel case:

$$\begin{aligned} x_1 &= 0.99s + n_1 \\ x_2 &= s + n_2. \end{aligned} \quad (14)$$

Here s is the CMB, x_i is the i^{th} channel of the data, and n_i is the foregrounds plus instrument noise. The calibration coefficients are equal to one and a calibration error of one percent has been considered in the first channel. If the signal-to-noise ratio is large enough, *e.g.* $n_i/s \ll 0.99$, then the noise is negligible in the observed maps

$$\begin{aligned} x_1 &\approx 0.99s \\ x_2 &\approx s. \end{aligned} \quad (15)$$

The ILC estimate of the CMB thus reduces in that case to

$$\hat{s} \approx 100x_1 - 99x_2, \quad (16)$$

where the weights satisfy the constraint $100 - 99 = 1$, which would guarantee the CMB conservation if the calibration

was correctly estimated. Consequently, the CMB estimate is of minimum variance since $E(\hat{s}^2) \approx 0$, but of course completely removes the expected input CMB, rendering the ILC totally irrelevant.

We may explain the process as follows. In presence of a calibration error in one channel the ILC algorithm minimizes the variance of

$$\hat{s} = (0.99w_1 + w_2)s + w_1n_1 + w_2n_2. \quad (17)$$

We can contrast this what we would get without calibration errors,

$$\hat{s} = (w_1 + w_2)s + w_1n_1 + w_2n_2. \quad (18)$$

With the constraint that $w_1 + w_2 = 1$, the contribution of the CMB signal to \hat{s} is always s . This indicates that the weights will take whatever values they need to take to minimize the contribution of the noise.

However, in the presence of calibration errors, it becomes possible for the contribution of s to \hat{s} to vary depending upon the choice of weights, indicating that a minimization of the variance of \hat{s} will introduce some competition between minimizing $(0.99w_1 + w_2)s$ and minimizing $w_1n_1 + w_2n_2$. For the following weights

$$\begin{aligned} w_1 &= 100, \\ w_2 &= -99, \end{aligned} \quad (19)$$

the contribution of the CMB to \hat{s} will be identically zero. This is what the ILC produces in the limit of the signal-to-noise ratio becoming very large with respect to the calibration error. In the opposite limit, that of small signal-to-noise ratio, it is the minimization of the second term, $w_1n_1 + w_2n_2$, that drives the minimization of \hat{s} , which mimics the behavior under the assumption of no calibration error.

4.5 The case of Planck

In table 1 we present the results of ten simulations of the sky with an ILC estimation of the CMB in presence of 0.1 %, 0.5 % and 1 % calibration errors for the Planck experiment (9 frequency channels).

For 1 % we observe a significant bias affecting the CMB reconstruction by ILC. The multiplicative factor $\alpha = 0.665$ (table 1) indicates that the CMB estimate eliminates roughly 33 % of the input CMB. The high sensitivity of Planck means a large signal-to-noise ratio, comparable to the inverse of the calibration error, which leads to a poorly extraction of the CMB by ILC, as expected from the formula (12). For 0.5 % calibration errors, 15 % of CMB is eliminated by the ILC estimation. Finally for 0.1 % calibration errors, 1 % of CMB is eliminated by the ILC estimation, which is nevertheless ten times the calibration error – and clearly not acceptable for precision cosmology with Planck.

4.6 The case of WMAP

In table 2 we present the results of ten simulations of the sky with an ILC estimation of the CMB in presence of 1 % calibration errors for the WMAP experiment. We observe a negligible bias affecting the CMB reconstruction by ILC. The multiplicative factor $\alpha \approx 0.99$ (table 2) indicates that the percentage of eliminated input CMB by ILC is for WMAP

[htbp]

<i>Planck</i>	1 %	0.5 %	0.1 %
mult. factor α	0.66500	0.85258	0.99237
add. error $E(c(p))$ (mK)	6.208e-2	3.455e-2	1.845e-2
$E(c(p)^2)$ (mK ²)	1.231e-2	3.46e-3	5.6e-4
$E((\hat{s} - s)^2)$ (mK ²)	4.26e-3	1.91e-3	5.5e-4
$E(s \cdot (\hat{s} - s))$ (mK ²)	-3.26e-3	-1.18e-3	-1.3e-4
$E(s^2)$ (mK ²)	7.42e-3	7.42e-3	7.42e-3
$E(\hat{s}^2)$ (mK ²)	5.16e-3	6.99e-3	7.71e-3

Table 1. ILC reconstruction errors for Planck in presence of 1 %, 0.5 % and 0.1 % calibration errors.

[htbp]

<i>WMAP</i>	1 %
mult. factor α	0.98709
add. error $E(c(p))$ (mK)	1.129e-2
$E(c(p)^2)$ (mK ²)	6.9e-4
$E((\hat{s} - s)^2)$ (mK ²)	6.5e-4
$E(s \cdot (\hat{s} - s))$ (mK ²)	-2.4e-4
$E(s^2)$ (mK ²)	5.15e-3
$E(\hat{s}^2)$ (mK ²)	5.33e-3

Table 2. ILC reconstruction errors for WMAP in presence of 1 % calibration errors.

of order of the calibration error, *i.e.* 1 %, as expected from formula (12) when the signal-to-noise ratio is small enough. The sensitivity of WMAP is small enough to render the ILC estimation of the CMB insensitive to calibration errors.

4.7 Actual WMAP ILC

The above result for WMAP was obtained assuming that the ILC is performed on the masked sky of figure 1. In fact, ILC weights used by the WMAP team have been computed in a different way, by subdividing the sky into twelve regions. Since the value of their weights are known, as well as the mean calibration error, we may easily evaluate the error of the reconstruction performed by the WMAP team.

The order of magnitude of the ILC weights w_i^{WMAP} computed by the WMAP team is comprised between 10^{-2} and 3 (Hinshaw et al., 2007) and the relative calibration errors have been estimated by the WMAP team to be of the order of $\delta_{a,i} \sim 0.2\%$.

In the subdivision of the sky by the WMAP team the region zero (Hinshaw et al., 2007) corresponds to the part of the sky outside the galaxy and thus dominated by the CMB signal. A priori, since the signal-to-noise ratio is the highest in that high galactic latitude region, one might expect the

effect of the calibration errors to be large. This is not the case, however.

We may estimate the maximum percentage of eliminated CMB in the region zero as follows:

$$\begin{aligned}
|1 - \alpha| &= \left| \sum_i w_i^{\text{WMAP}} \delta_{a_i} \right| \\
&\leq 0.002 \sum_i |w_i^{\text{WMAP}}| \\
&\leq 7 \cdot 10^{-3} = 0.7\%,
\end{aligned} \tag{20}$$

where w_i^{WMAP} are the ILC weights computed by the WMAP team in the region zero (Hinshaw et al., 2007). Therefore, the maximum percentage of eliminated CMB has the order of magnitude of the calibration error, *i.e.* few $\times 10^{-1}$ %, which is small.⁴ So the multiplicative factor for the actual WMAP ILC in presence of 0.2 % calibration errors is close to one, with a minor loss of CMB power:

$$\alpha \geq 0.993.$$

Interestingly, the ILC weights used at high galactic latitude by the WMAP team (Hinshaw et al., 2007) have been computed in a low galactic latitude region of the sky, where the signal-to-noise ratio is sufficiently small. This certainly explains why the ILC weights are close to those expected with no calibration errors and why the multiplicative factor is close to one. Therefore the calibration uncertainties do not have a strong impact on the ILC weights computed in the WMAP third year data release. The bias due to calibration errors is negligible.

The price paid for this, as emphasized by Delabrouille et al. (2009), is that at high galactic latitude the WMAP weights are chosen to cancel galactic foregrounds rather than instrumental noise, a sub-optimal choice away from the galaxy, particularly for small scales.

4.8 Other ILC performed on WMAP

Several authors have used a version of the ILC to analyze WMAP data. The present paper warns the users of the cor-

⁴ It should be noticed that this bound is a rough estimation since we do not have access to the real value of the calibration error for each frequency channel.

responding data sets that in presence of calibration errors, some CMB power may be lost in the maps obtained. Further investigation would be needed to evaluate the exact impact for each individual recovered CMB map.

4.9 De-biasing

A natural question to ask is whether, since the effect of calibration errors is to introduce a loss of CMB power, it would not be possible to correct from this effect and ‘recalibrate’ a posteriori in some way.

First of all, this can not be the optimal solution, as the noise contribution to the total error would be increased accordingly. The proper solution would be to get the right calibration beforehand. As we can see from figure 5 that the variance of α seems to be of order $1 - \alpha$. This indicates that the maximum improvement on the level of the CMB is to reduce the expectation value of $|1 - \alpha|$ by around a factor of two. As $1 - \alpha$ becomes very large very quickly, this will not help when the calibration is not already very good compared to the signal to noise ratio.

Finally, even the knowledge of the expectation value of α is not very easy to get. Simulations give an estimate of its amplitude, but the actual value may depend on details, for which simulations are not guaranteed to be representative.

Hence, we leave this question open for further investigations.

4.10 Impact of the number of channels

Tests performed varying the number of channels used to perform the ILC with Planck data show that ILC does better with calibration errors if fewer channels are used. To add new data, but end up with worse estimation of the desired products, indicates that the new data is not being used effectively, to say the least.

The reason for this degradation of the performance of the ILC when more channels are added is easy to understand. As discussed in section 4.3, the ILC can erroneously cancel out part of the CMB if the signal to noise ratio is larger than the inverse of the calibration error, i.e. if

$$\sigma^2 \delta_a^t R_n^{-1} \delta_a \gg 1. \quad (21)$$

As R_n^{-1} and R_n are symmetric matrices, they can be diagonalized, and we can write:

$$R_n^{-1} = O^t D_n^{-1} O,$$

where O is an orthonormal matrix, and D_n^{-1} a diagonal matrix. The condition of eq. (21) then becomes:

$$\sigma^2 (O \delta_a)^t D_n^{-1} (O \delta_a) \gg 1. \quad (22)$$

Matrix O preserves the norm, and thus elements of $O \delta_a$ are of the same order as those of δ_a . It then suffices that one of the eigenvalues of D_n be small for $\sigma^2 \delta_a^t R_n^{-1} \delta_a$ to be large, causing the CMB power loss discussed in this paper.

Now recalling that R_n is the covariance matrix of noise + foregrounds, it is easy to understand why more channels cause more problems with Planck. Foregrounds are significantly brighter than the noise, and comparable in amplitude to the CMB over a fraction of the sky. If they span a space of dimension equal or greater than the number of channels,

matrix D_n will have no small eigenvalue. If on the other hand they span a space of dimension less than the number of channels, matrix D_n will have at least one small eigenvalue, generating the ‘CMB loss’ problem.

Physically, this is understood in the following way: if there are few channels, the minimization of the variance of the ILC linear combination will be achieved by canceling foregrounds primarily. If however there are additional channels which are not needed to cancel out the foregrounds, the extra channels leave more freedom for the ILC weights to adjust themselves so as to cancel part of the CMB as well.

5 CONCLUSION

The primary conclusion of our work is that some care is required for performing component separation in presence of calibration errors, in particular for sensitive multichannel instruments such as Planck. We have shown that two different component separation algorithms, FastICA and ILC, behave very differently in the presence of calibration errors. FastICA is completely unaffected, while ILC can become biased by a significant amount with even small calibration errors. We propose that those attempting to make use of these or other component separation techniques pay close attention to how calibration errors affect their results. Some techniques will doubtlessly be completely unaffected, as FastICA was, while others may be very sensitive like ILC.

We also note that due to the fact that ILC in the presence of sufficient calibration errors biases the variance of the CMB low, and because we have a lower limit upon the variance of the CMB from WMAP, through its measurement of the CMB power spectrum up to about $\ell = 900$, the variance of the ILC output may prove a useful diagnostic test if the calibration of Planck was performed well. The ability to use this as a cross-check on calibration also indicates that for a Planck-style mission we expect to recover, at a minimum, around 0.1%-0.2% relative calibration error. The reasoning for this is that if the calibration error is worse, then ILC will produce a CMB map that is of lower-variance than a similar map from WMAP, which, in turn, tells us that the calibration wasn’t very good. If we have information that the calibration wasn’t as good as it could have been, then it is reasonable to expect that it is possible to improve said calibration.

Note that even though FastICA is not biased where ILC is, it is not clear that FastICA is better. ILC does seem to produce lower errors in extracting the CMB, as seen in figures 2 and 3. The biasing is troubling, but ILC retains lower extraction error up to somewhere between 0.1% and 0.2% calibration error, at least at high galactic latitudes. If the calibration error is good enough, then we still expect ILC to remain a very useful method for extracting the CMB.

ACKNOWLEDGMENTS

We would like to thank Carlo Baccigalupi, Jean-François Cardoso, Maude Le Jeune, and Radek Stompfor for useful conversations related to this work.

APPENDIX A: ANALYTIC ANALYSIS OF ILC

In this appendix we analytically derive the bias of the ILC estimator generated by calibration errors, and look at the impact of the signal-to-noise ratio on this bias. In particular we show that, even in presence of small calibration errors, the ILC tends to poorly extract the CMB if the signal-to-noise ratio is large.

Review of ILC

We model the data as:

$$\mathbf{x}(p) = \mathbf{a} s(p) + \mathbf{n}(p), \quad (\text{A1})$$

where $\mathbf{x}(p)$ is the vector of the observed data at the pixel (or harmonic mode, or needlet coefficient) p for the set of frequency channels, $s(p)$ is the CMB signal, and $\mathbf{n}(p)$ is the vector of corresponding noise (including both foregrounds contaminants and instrumental noise) for the set of frequency channels. \mathbf{a} is a vector which contains the frequency scaling of the component, so that in the case of CMB with no calibration errors one has $\mathbf{a} = (1, 1, \dots, 1)$. In the following we omit the index p .

We use σ^2 and \mathbf{R}_n respectively to denote the variance of the CMB signal s and the covariance matrix of the noise \mathbf{n} (including foregrounds), and we assume that s and \mathbf{n} are independent such that the covariance matrix of the observed maps is $\mathbf{R}_x = (\mathbf{R}_n + \sigma^2 \mathbf{a} \mathbf{a}^t)$. The ILC implements an approximation of the ideal filter

$$\hat{s} = \frac{\mathbf{a}^t \mathbf{R}_x^{-1} \mathbf{x}}{\mathbf{a}^t \mathbf{R}_x^{-1} \mathbf{a}}, \quad (\text{A2})$$

which is an unbiased minimum variance estimate of s . In practice, the covariance \mathbf{R}_x used in the ILC is an empirical estimate on a sample of finite size, and thus slightly differs from its ensemble average ($\hat{\mathbf{R}}_x = \mathbf{R}_x + \Delta_x$). This induces a bias in the variance of the ILC, as shown by Delabrouille et al. (2009). In this appendix we assume $\hat{\mathbf{R}}_x = \mathbf{R}_x$ to investigate the bias that stems from errors in calibration alone ($\hat{\mathbf{a}} = \mathbf{a} + \boldsymbol{\delta}_a$).

Bias due to calibration errors

An imperfectly estimated frequency scaling vector \mathbf{a} includes calibration errors $\boldsymbol{\delta}_a$ which introduce a discrepancy between the observed data and the ILC weights that are used to reconstruct the CMB. This discrepancy is expected to be responsible for a bias in the reconstruction. Due to calibration errors $\boldsymbol{\delta}_a$ the observed map is modified as

$$\begin{aligned} \mathbf{x} &= (\mathbf{a} + \boldsymbol{\delta}_a) s + \mathbf{n}, \\ \mathbf{R}_x &= \mathbf{R}_n + \sigma^2 (\mathbf{a} + \boldsymbol{\delta}_a) (\mathbf{a} + \boldsymbol{\delta}_a)^t, \end{aligned} \quad (\text{A3})$$

such that the ILC estimate becomes⁵

$$\hat{s} = \frac{\mathbf{a}^t [\mathbf{R}_n + \sigma^2 (\mathbf{a} + \boldsymbol{\delta}_a) (\mathbf{a} + \boldsymbol{\delta}_a)^t]^{-1}}{\mathbf{a}^t [\mathbf{R}_n + \sigma^2 (\mathbf{a} + \boldsymbol{\delta}_a) (\mathbf{a} + \boldsymbol{\delta}_a)^t]^{-1} \mathbf{a}} ((\mathbf{a} + \boldsymbol{\delta}_a) s + \mathbf{n}). \quad (\text{A4})$$

Making use of the inversion formula:

$$\mathbf{R}_x^{-1} = [\mathbf{R}_n + \sigma^2 (\mathbf{a} + \boldsymbol{\delta}_a) (\mathbf{a} + \boldsymbol{\delta}_a)^t]^{-1} = \mathbf{R}_n^{-1} - \sigma^2 \frac{\mathbf{R}_n^{-1} (\mathbf{a} + \boldsymbol{\delta}_a) (\mathbf{a} + \boldsymbol{\delta}_a)^t \mathbf{R}_n^{-1}}{1 + \sigma^2 (\mathbf{a} + \boldsymbol{\delta}_a)^t \mathbf{R}_n^{-1} (\mathbf{a} + \boldsymbol{\delta}_a)}, \quad (\text{A5})$$

we obtain the weights \mathbf{w} of the ILC ($\hat{s} = \mathbf{w}^t \mathbf{x}$) as

$$\mathbf{w}^t = \frac{\mathbf{a}^t \mathbf{R}_n^{-1} + \sigma^2 \mathbf{a}^t \mathbf{R}_n^{-1} (\mathbf{a}^t \mathbf{R}_n^{-1} \boldsymbol{\delta}_a + \boldsymbol{\delta}_a^t \mathbf{R}_n^{-1} \boldsymbol{\delta}_a) - \sigma^2 \boldsymbol{\delta}_a^t \mathbf{R}_n^{-1} (\mathbf{a}^t \mathbf{R}_n^{-1} \mathbf{a} + \mathbf{a}^t \mathbf{R}_n^{-1} \boldsymbol{\delta}_a)}{\mathbf{a}^t \mathbf{R}_n^{-1} \mathbf{a} + \sigma^2 (\mathbf{a}^t \mathbf{R}_n^{-1} \mathbf{a}) (\boldsymbol{\delta}_a^t \mathbf{R}_n^{-1} \boldsymbol{\delta}_a) - \sigma^2 (\mathbf{a}^t \mathbf{R}_n^{-1} \boldsymbol{\delta}_a)^2}. \quad (\text{A6})$$

In the absence of calibration errors ($\boldsymbol{\delta}_a = 0$) we recover the standard ILC weights:

$$\mathbf{w}^t|_{\boldsymbol{\delta}_a=0} = \frac{\mathbf{a}^t \mathbf{R}_n^{-1}}{\mathbf{a}^t \mathbf{R}_n^{-1} \mathbf{a}} = \frac{\mathbf{a}^t \mathbf{R}_x^{-1}}{\mathbf{a}^t \mathbf{R}_x^{-1} \mathbf{a}}, \quad (\text{A7})$$

where the second equality⁶ comes from the inversion formula (A5). We see that the presence of calibration errors induces a departure from the standard ILC weights through correction terms which explicitly depend on the signal-to-noise ratio $\sigma^2 \mathbf{R}_n^{-1}$. Typically if the signal-to-noise ratio is much smaller than the inverse of the calibration error squared (e.g. $\boldsymbol{\delta}_a^t \sigma^2 \mathbf{R}_n^{-1} \boldsymbol{\delta}_a \ll 1$) then the calibration errors will have little impact and the standard ILC weights are relevant. Else if the signal-to-noise ratio becomes comparable to the inverse of the calibration error squared then the impact of calibration errors may be more dramatic

⁵ It should be noted that the derivation would have been of course completely equivalent if we had considered calibration errors into the ILC weights instead of into the data.

⁶ In practice we have only access to the covariance matrix \mathbf{R}_x of the observed maps but not to the noise covariance matrix \mathbf{R}_n (including foregrounds) for constructing the ILC estimate. But theoretically the both representations of the ILC estimate are identical.

on the CMB reconstruction since the variance of the ILC may be much lower than the true CMB. In the exact expression (A6) we intentionally conserved second order terms in δ_a because they play a role of regularization terms when the signal-to-noise ratio $\sigma^2 \mathbf{R}_n^{-1}$ goes to infinity.

As a simple illustration let us apply the above result to the following example with two frequency channels and a diagonal noise covariance matrix:

$$\begin{aligned} x_1 &= 0.99s + n_1 \\ x_2 &= s + n_2. \end{aligned} \quad (\text{A8})$$

Here the calibration error is one percent. We note $\sigma^2 = E(s^2)$, $\mathbf{R}_n = \text{diag}[\sigma_1^2, \sigma_2^2]$, where $\sigma_i^2 = E(n_i^2)$. In this example $\mathbf{a}^t = (1, 1)$ and $\delta_a^t = (-0.01, 0)$ so that the expression (A6) of $\mathbf{w}^t = (w_1, w_2)$ reduces to

$$w_1 = \frac{\frac{\sigma_2^2}{\sigma^2} - \delta_{a1}}{\frac{\sigma_1^2 + \sigma_2^2}{\sigma^2} + \delta_{a1}^2} \quad (\text{A9})$$

$$w_2 = \frac{\frac{\sigma_1^2}{\sigma^2} + (1 + \delta_{a1})\delta_{a1}}{\frac{\sigma_1^2 + \sigma_2^2}{\sigma^2} + \delta_{a1}^2}. \quad (\text{A10})$$

If the signal-to-noise ratio becomes very large (*i.e.* $\sigma_i^2/\sigma^2 \rightarrow 0$) then $w_1 \approx -1/\delta_{a1} = 100$ and $w_2 \approx (1 + \delta_{a1})/\delta_{a1} = -99$, so that the output CMB vanishes $\hat{s} \approx 100x_1 - 99x_2 \approx 100n_1 - 99n_2 \approx 0$ when the noise is negligible. If the signal-to-noise ratio becomes very small then $w_1 \approx \sigma_2^2/(\sigma_1^2 + \sigma_2^2)$ and $w_2 \approx \sigma_1^2/(\sigma_1^2 + \sigma_2^2)$, which is the standard least mean square solution.

The ILC estimate is given by

$$\begin{aligned} \hat{s} &= \mathbf{w}^t (\mathbf{a} + \delta_a) s + \mathbf{w}^t \mathbf{n}, \\ \hat{s} &= \frac{\mathbf{a}^t \mathbf{R}_n^{-1} \mathbf{a} + \mathbf{a}^t \mathbf{R}_n^{-1} \delta_a}{\mathbf{a}^t \mathbf{R}_n^{-1} \mathbf{a} + \sigma^2 (\mathbf{a}^t \mathbf{R}_n^{-1} \mathbf{a}) (\delta_a^t \mathbf{R}_n^{-1} \delta_a) - \sigma^2 (\mathbf{a}^t \mathbf{R}_n^{-1} \delta_a)^2} s + \mathbf{w}^t \mathbf{n}, \end{aligned} \quad (\text{A11})$$

We assume $E(\mathbf{n}) = 0$, the ILC estimate is thus biased as

$$E(\hat{s}) = \frac{\mathbf{a}^t \mathbf{R}_n^{-1} \mathbf{a} + \mathbf{a}^t \mathbf{R}_n^{-1} \delta_a}{\mathbf{a}^t \mathbf{R}_n^{-1} \mathbf{a} + \sigma^2 (\mathbf{a}^t \mathbf{R}_n^{-1} \mathbf{a}) (\delta_a^t \mathbf{R}_n^{-1} \delta_a) - \sigma^2 (\mathbf{a}^t \mathbf{R}_n^{-1} \delta_a)^2} E(s). \quad (\text{A12})$$

We see that in the limit of small signal-to-noise ratio, $\sigma^2 (\mathbf{R}_n^{-1})_{ij} \ll 1$, the bias is of order of magnitude of the calibration error: $E(s) \mathbf{a}^t \mathbf{R}_n^{-1} \delta_a / \mathbf{a}^t \mathbf{R}_n^{-1} \mathbf{a}$. Whereas if $\sigma^2 (\mathbf{R}_n^{-1})_{ij} \gg 1$ then the bias is accentuated since $E(\hat{s}) \rightarrow 0$.

Let us compute the mean value of the error $d = \hat{s} - s$ (assuming $E(\mathbf{n}) = 0$):

$$\begin{aligned} E(d) &= E(\mathbf{w}^t (\mathbf{a} + \delta_a) s - s) \\ &= \frac{\mathbf{a}^t \mathbf{R}_n^{-1} \delta_a - \sigma^2 [(\mathbf{a}^t \mathbf{R}_n^{-1} \mathbf{a}) (\delta_a^t \mathbf{R}_n^{-1} \delta_a) - (\mathbf{a}^t \mathbf{R}_n^{-1} \delta_a)^2]}{\mathbf{a}^t \mathbf{R}_n^{-1} \mathbf{a} + \sigma^2 [(\mathbf{a}^t \mathbf{R}_n^{-1} \mathbf{a}) (\delta_a^t \mathbf{R}_n^{-1} \delta_a) - (\mathbf{a}^t \mathbf{R}_n^{-1} \delta_a)^2]} E(s), \end{aligned} \quad (\text{A13})$$

so that $E(d) \rightarrow -E(s)$ when $\sigma^2 (\mathbf{R}_n^{-1})_{ij} \gg 1$, and $E(d) \rightarrow 0$ when $\sigma^2 (\mathbf{R}_n^{-1})_{ij} \ll 1$ and $\delta_a \ll \mathbf{a}$.

In the same way the cross correlation $E(s d)$ of the error of the reconstruction with the CMB signal

$$E(s d) = \frac{\mathbf{a}^t \mathbf{R}_n^{-1} \delta_a - \sigma^2 [(\mathbf{a}^t \mathbf{R}_n^{-1} \mathbf{a}) (\delta_a^t \mathbf{R}_n^{-1} \delta_a) - (\mathbf{a}^t \mathbf{R}_n^{-1} \delta_a)^2]}{\mathbf{a}^t \mathbf{R}_n^{-1} \mathbf{a} + \sigma^2 [(\mathbf{a}^t \mathbf{R}_n^{-1} \mathbf{a}) (\delta_a^t \mathbf{R}_n^{-1} \delta_a) - (\mathbf{a}^t \mathbf{R}_n^{-1} \delta_a)^2]} \sigma^2, \quad (\text{A14})$$

may vanish only if $\sigma^2 (\mathbf{R}_n^{-1})_{ij} \ll 1$. If the signal-to-noise ratio becomes large enough then $E(s d) \rightarrow -\sigma^2$, giving evidence of the cancellation of the CMB output.

We may also compute the variance of the error. Since the CMB and the noise are uncorrelated we get

$$\begin{aligned} E(d^2) &= (\mathbf{w}^t \delta_a)^2 \sigma^2 + \mathbf{w}^t \mathbf{R}_n \mathbf{w} \\ &\approx \left(\frac{\mathbf{a}^t \mathbf{R}_n^{-1} \delta_a - \sigma^2 [(\mathbf{a}^t \mathbf{R}_n^{-1} \mathbf{a}) (\delta_a^t \mathbf{R}_n^{-1} \delta_a) - (\mathbf{a}^t \mathbf{R}_n^{-1} \delta_a)^2]}{\mathbf{a}^t \mathbf{R}_n^{-1} \mathbf{a} + \sigma^2 [(\mathbf{a}^t \mathbf{R}_n^{-1} \mathbf{a}) (\delta_a^t \mathbf{R}_n^{-1} \delta_a) - (\mathbf{a}^t \mathbf{R}_n^{-1} \delta_a)^2]} \right)^2 \sigma^2 \\ &\quad + \frac{\mathbf{a}^t \mathbf{R}_n^{-1} \mathbf{a} + \sigma^2 (2 + \sigma^2 \mathbf{a}^t \mathbf{R}_n^{-1} \mathbf{a}) [(\mathbf{a}^t \mathbf{R}_n^{-1} \mathbf{a}) (\delta_a^t \mathbf{R}_n^{-1} \delta_a) - (\mathbf{a}^t \mathbf{R}_n^{-1} \delta_a)^2]}{(\mathbf{a}^t \mathbf{R}_n^{-1} \mathbf{a} + \sigma^2 [(\mathbf{a}^t \mathbf{R}_n^{-1} \mathbf{a}) (\delta_a^t \mathbf{R}_n^{-1} \delta_a) - (\mathbf{a}^t \mathbf{R}_n^{-1} \delta_a)^2])^2}. \end{aligned} \quad (\text{A15})$$

Notice that the second term has been truncated at second order in δ_a . If $\sigma^2 (\mathbf{R}_n^{-1})_{ij} \ll 1$ then we recover the standard reconstruction error with no calibration error: $E(d^2) \approx 1/(\mathbf{a}^t \mathbf{R}_n^{-1} \mathbf{a})$, as computed by Delabrouille et al. (2009). If the

signal-to-noise ratio becomes large enough then $\mathbf{w}^t R_n \mathbf{w}$ becomes negligible compared to the first term $(\mathbf{w}^t \boldsymbol{\delta}_a)^2 \sigma^2$ such that $E(d^2) \approx \sigma^2$, again giving evidence of the cancellation of the CMB output.

REFERENCES

- Bedini, L., Herranz, D., Salerno, E., Baccigalupi, C., Kuruouglu, E. E., & Tonazzini, A. 2005, *EURASIP Journal on Applied Signal Processing*, Vol. 2005 (Applications of Signal Processing in Astrophysics and Cosmology), Guest Editors Kuruouglu E. E. and Baccigalupi, C., p. 2400-2412, 2005, 2400
- Benoît, A., Ade, P., Amblard, A., Ansari, R., Aubourg, É., Bargot, S., Bartlett, J. G., Bernard, J.-P., Bhatia, R. S., Blanchard, A., Bock, J. J., Boscaleri, A., Bouchet, F. R., Bourrachot, A., Camus, P., Couchot, F., de Bernardis, P., Delabrouille, J., Désert, F.-X., Doré, O., Douspis, M., Dumoulin, L., Dupac, X., Filliatre, P., Fosalba, P., Ganga, K., Gannaway, F., Gautier, B., Giard, M., Giraud-Héraud, Y., Gispert, R., Guglielmi, L., Hamilton, J.-C., Hanany, S., Henrot-Versillé, S., Kaplan, J., Lagache, G., Lamarre, J.-M., Lange, A. E., Macías-Pérez, J. F., Madet, K., Maffei, B., Magneville, C., Marrone, D. P., Masi, S., Mayet, F., Murphy, A., Naraghi, F., Nati, F., Patanchon, G., Perrin, G., Piat, M., Ponthieu, N., Prunet, S., Puget, J.-L., Renault, C., Rosset, C., Santos, D., Starobinsky, A., Strukov, I., Sudiwala, R. V., Teyssier, R., Tristram, M., Tucker, C., Vanel, J.-C., Vibert, D., Wakui, E., & Yvon, D. 2003, *A&A*, 399, L25
- Bersanelli, M., & Mandolesi, N. 2000, *Astrophysical Letters Communications*, 37, 171
- Bobin, J., Moudden, Y., Starck, J.-L., Fadili, J., & Aghanim, N. 2008, *Statistical Methodology*, 5, 307
- Bonaldi, A., Bedini, L., Salerno, E., Baccigalupi, C., & de Zotti, G. 2006, *MNRAS*, 373, 271
- Bonaldi, A., Ricciardi, S., Leach, S., Stivoli, F., Baccigalupi, C., & de Zotti, G. 2007, *MNRAS*, 382, 1791
- Cardoso, J.-F., Le Jeune, M., Delabrouille, J., Betoule, M., & Patanchon, G. 2008, *IEEE Journal of Selected Topics in Signal Processing*, vol. 2, issue 5, pp. 735-746, 2, 735
- Delabrouille, J., & Cardoso, J. . 2007, *ArXiv Astrophysics e-prints*, arXiv:astro-ph/0702198
- Delabrouille, J., Cardoso, J.-F., Le Jeune, M., Betoule, M., Fay, G., & Guilloux, F. 2009, *A&A*, 493, 835
- Delabrouille, J., Cardoso, J.-F., & Patanchon, G. 2003, *MNRAS*, 346, 1089
- Eriksen, H. K., Banday, A. J., Górski, K. M., & Lilje, P. B. 2004, *ApJ*, 612, 633
- Fixsen, D. J., Hinshaw, G., Bennett, C. L., & Mather, J. C. 1997, *ApJ*, 486, 623
- Hinshaw, G., Nolta, M. R., Bennett, C. L., Bean, R., Doré, O., Greason, M. R., Halpern, M., Hill, R. S., Jarosik, N., Kogut, A., Komatsu, E., Limon, M., Odegard, N., Meyer, S. S., Page, L., Peiris, H. V., Spergel, D. N., Tucker, G. S., Verde, L., Weiland, J. L., Wollack, E., & Wright, E. L. 2007, *ApJS*, 170, 288
- Hyvärinen, A. 1999, *IEEE Transactions on Neural Networks*, 10, 626
- Kim, J., Naselsky, P., & Christensen, P. R. 2009, *Phys. Rev. D*, 79, 023003
- Komatsu, E., Dunkley, J., Nolta, M. R., Bennett, C. L., Gold, B., Hinshaw, G., Jarosik, N., Larson, D., Limon, M., Page, L., Spergel, D. N., Halpern, M., Hill, R. S., Kogut, A., Meyer, S. S., Tucker, G. S., Weiland, J. L., Wollack, E., & Wright, E. L. 2009, *ApJS*, 180, 330
- Lamarre, J. M., Ade, P. R., Benoît, A., de Bernardis, P., Bock, J., Bouchet, F., Bradshaw, T., Charra, J., Church, S., Couchot, F., Delabrouille, J., Efstathiou, G., Giard, M., Giraud-Héraud, Y., Gispert, R., Griffin, M., Lange, A., Murphy, A., Pajot, F., Puget, J. L., & Ristorcelli, I. 2000, *Astrophysical Letters Communications*, 37, 161
- Leach, S. M., Cardoso, J.-F., Baccigalupi, C., Barreiro, R. B., Betoule, M., Bobin, J., Bonaldi, A., Delabrouille, J., de Zotti, G., Dickinson, C., Eriksen, H. K., González-Nuevo, J., Hansen, F. K., Herranz, D., Le Jeune, M., López-Caniego, M., Martínez-González, E., Massardi, M., Melin, J.-B., Miville-Deschênes, M.-A., Patanchon, G., Prunet, S., Ricciardi, S., Salerno, E., Sanz, J. L., Starck, J.-L., Stivoli, F., Stolyarov, V., Stompor, R., & Vielva, P. 2008, *A&A*, 491, 597
- MacTavish, C. J., Ade, P. A. R., Bock, J. J., Bond, J. R., Borrill, J., Boscaleri, A., Cabella, P., Contaldi, C. R., Crill, B. P., de Bernardis, P., De Gasperis, G., de Oliveira-Costa, A., De Troia, G., di Stefano, G., Hivon, E., Jaffe, A. H., Jones, W. C., Kisner, T. S., Lange, A. E., Lewis, A. M., Masi, S., Mauskopf, P. D., Melchiorri, A., Montroy, T. E., Natoli, P., Netterfield, C. B., Pascale, E., Piacentini, F., Pogosyan, D., Polenta, G., Prunet, S., Ricciardi, S., Romeo, G., Ruhl, J. E., Santini, P., Tegmark, M., Veneziani, M., & Vittorio, N. 2006, *ApJ*, 647, 799
- Maino, D., Donzelli, S., Banday, A. J., Stivoli, F., & Baccigalupi, C. 2006, *ArXiv Astrophysics e-prints*, arXiv:astro-ph/0609228
- Maino, D., Farusi, A., Baccigalupi, C., Perrotta, F., Banday, A. J., Bedini, L., Burigana, C., De Zotti, G., Górski, K. M., & Salerno, E. 2002, *MNRAS*, 334, 53
- Patanchon, G., Cardoso, J.-F., Delabrouille, J., & Vielva, P. 2005, *MNRAS*, 364, 1185
- QUaD collaboration: C. Pryke, Ade, P., Bock, J., Bowden, M., Brown, M. L., Cahill, G., Castro, P. G., Church, S., Culverhouse, T., Friedman, R., Ganga, K., Gear, W. K., Gupta, S., Hinderks, J., Kovac, J., Lange, A. E., Leitch, E., Melhuish, S. J., Memari, Y., Murphy, J. A., Orlando, A., Schwarz, R., O’Sullivan, C., Piccirillo, L., Rajguru, N., Rusholme, B., Taylor, A. N., Thompson, K. L., Turner, A. H., Wu, E. Y. S., & Zemcov, M. 2008, *ArXiv e-prints*, arXiv:0805.1944
- Rebolo, R., Battye, R. A., Carreira, P., Cleary, K., Davies, R. D., Davis, R. J., Dickinson, C., Genova-Santos, R., Grainge, K., Gutiérrez, C. M., Hafez, Y. A., Hobson, M. P., Jones, M. E., Kneissl, R., Lancaster, K., Lasenby, A., Leahy, J. P., Maisinger, K., Pooley, G. G., Rajguru, N., Rubiño-Martin, J. A., Saunders, R. D. E., Savage, R. S., Scaife, A., Scott, P. F., Slosar, A., Sosa Molina, P., Taylor, A. C., Titterton, D., Waldram, E., Watson, R. A., & Wilkinson, A. 2004, *MNRAS*, 353, 747

- Reichardt, C. L., Ade, P. A. R., Bock, J. J., Bond, J. R., Brevik, J. A., Contaldi, C. R., Daub, M. D., Dempsey, J. T., Goldstein, J. H., Holzappel, W. L., Kuo, C. L., Lange, A. E., Lueker, M., Newcomb, M., Peterson, J. B., Ruhl, J., Runyan, M. C., & Staniszewski, Z. 2009, *ApJ*, 694, 1200
- Sievers, J. L., Mason, B. S., Weintraub, L., Achermann, C., Altamirano, P., Bond, J. R., Bronfman, L., Bustos, R., Contaldi, C., Dickinson, C., Jones, M. E., May, J., Myers, S. T., Oyarce, N., Padin, S., Pearson, T. J., Pospieszalski, M., Readhead, A. C. S., Reeves, R., Shepherd, M. C., Taylor, A. C., & Torres, S. 2009, ArXiv e-prints, arXiv:0901.4540
- Tauber, J. A. 2004, *Advances in Space Research*, 34, 491
- Tegmark, M., de Oliveira-Costa, A., & Hamilton, A. J. 2003, *Phys. Rev. D*, 68, 123523
- Tristram, M., Patanchon, G., Macías-Pérez, J. F., Ade, P., Amblard, A., Ansari, R., Aubourg, É., Benoît, A., Bernard, J.-P., Blanchard, A., Bock, J. J., Bouchet, F. R., Bourrachot, A., Camus, P., Cardoso, J.-F., Couchot, F., de Bernardis, P., Delabrouille, J., Désert, F.-X., Douspis, M., Dumoulin, L., Filliatre, P., Fosalba, P., Giard, M., Giraud-Héraud, Y., Gispert, R., Guglielmi, L., Hamilton, J.-C., Hanany, S., Henrot-Versillé, S., Kaplan, J., Lagache, G., Lamarre, J.-M., Lange, A. E., Madet, K., Maffei, B., Magneville, C., Masi, S., Mayet, F., Nati, F., Perdereau, O., Plaszczyński, S., Piat, M., Ponthieu, N., Prunet, S., Renault, C., Rosset, C., Santos, D., Vibert, D., & Yvon, D. 2005, *A&A*, 436, 785